doi:10.2533/chimia.2015.737 Chimia 69 (2015) 737–740

Stress-induced Ageing of Lithium-Ion Batteries

Marcel Held* and Urs Sennhauser

Abstract: Lithium-ion batteries are well established for use in portable consumer products and are increasingly used in high power electro-mobility and photovoltaic storage applications. In hybrid and plug-in electric vehicles degradation and useful lifetime at standard operation conditions are critical parameters in addition to performance and safety. Here stress-induced ageing of commercially available high power battery cells of the type A123 AHR32113M1 Ultra-B, consisting of a $LiFePO_4$ cathode and a graphite anode have been investigated. A usually accepted capacity loss for electric vehicles of 20% was reached after 8560 stress profiles corresponding to a driving distance of almost 200'000 km. Cycling with a stress profile applying constant power corresponding to the average power and energy of a full stress profile and starting at 60% state of charge showed a much faster capacity loss. Electric impedance measurements show the dependence of the capacity loss and constant phase element at low frequency, indicating Li-ion diffusion blocking in the cathode. Microscopic analysis of anode, separator, and cathode, shows defect formation in bulk material and at interfaces.

Keywords: Electrochemical impedance spectroscopy · Li-ion batteries · Microscopy · Stress cycles

1. Introduction

Lithium-ion rechargeable batteries provide high volumetric and gravimetric energy and power density, have no memory effect and show very little self-discharge when not in use. Despite some early safety and lifetime concerns they are now well established for use in portable consumer electronic products and they are increasingly used in electro-mobility, energy storage, aerospace, and medical implants. Li-ion batteries, including cells and management electronics, are optimized for the various applications concerning performance, environmental conditions, load profile, useful lifetime, biocompatibility, and system reliability and costs. Despite extensive investigations in industrial and academic work[1–4] to identify degradation mechanisms of connectors, electrodes, electrolytes, separators, and various interfaces, standardized procedures for different applications have yet to be established.

In this study the focus lies on capacity loss for different stress cycles, state of charge (SOC) ranges, and storage periods. Electrochemical impedance spectroscopy and microscopy studies have been performed to investigate capacity loss and degradation processes. Adapting the battery power cycling to the worldwide harmonized light vehicles test procedure (WLTC) to electric vehicles allows an estimation of their total cruising range until 20% of the nominal capacity is lost.

2. Test and Electrical Measurement Procedures

In this work commercial high power battery cells of the type A123 AHR32113M1 Ultra-B, consisting of a $LiFePO_4$ cathode and a graphite anode were investigated. New battery cells exhibit a nominal voltage of 3.3 V, a capacity of 4.4 Ah, and a maximum discharge power of 550 W. This type of battery has been designed for hybrid power trains of light vehicles.[5] The full battery consists of 70 single cells in series to provide a total capacity of 1.04 kWh and a maximum power of 20 kW.

In order to study the capacity loss, rechargeable Li-ion cells are usually cycled by a complete charge and discharge process. For automotive applications, so-called worldwide harmonized light vehicles test procedures (WLTP) were developed to measure the real power consumption during drive cycles (WLTC).[6] In this work the WLTC driving cycle class 3 – comprising low, medium, high, and extra high speed parts – was used to derive the power stress profile of a single cell of the battery pack (Fig. 1). The maximum power is 284.5 W for charging and 356.8 W for discharging and the average power 80.56 W for charging and 55.52 W for discharging. The total time of the stress profile is 1800 seconds whereas 996 seconds are charging and 804 seconds discharging. In order to optimize the overall energy consumption of the hybrid power train and to keep the battery in a defined state the state of charge (SOC) of the cell is 60% (2.64 Ah) at beginning and end of the power stress cycle.

Cell 1 was aged with WLTC power stress cycles. During each cycle the cell fluctuates between 42% and 100% SOC. Intermediate characterization measurements were performed every 51 cycles.

For cell 2 the average power values of the WLTC procedure were used to first discharge the cell for 804 s and then charge it for 996 s. With this procedure the cell was completely discharged and charged, *i.e.* SOC fluctuated between 0 and 100%.

The average power values of the power stress profile were also taken for cell 3 and cell 4, but with modified time and SOC spans. Cell 3 was discharged and charged with 0.88 Ah between 40% and 60% SOC, whereas cell 4 was discharged and charged with 1.76 Ah between 20% and 60% SOC. Cells 3 and 4 had been stored for 10 months at 25 °C ambient temperature and were (over-) discharged. However they were revitalized by slow charging showing

*Correspondence: M. Held
Reliability Science and Technology Laboratory
Empa
Überlandstrasse 129
CH-8600 Dübendorf
E-mail: marcel.held@empa.ch

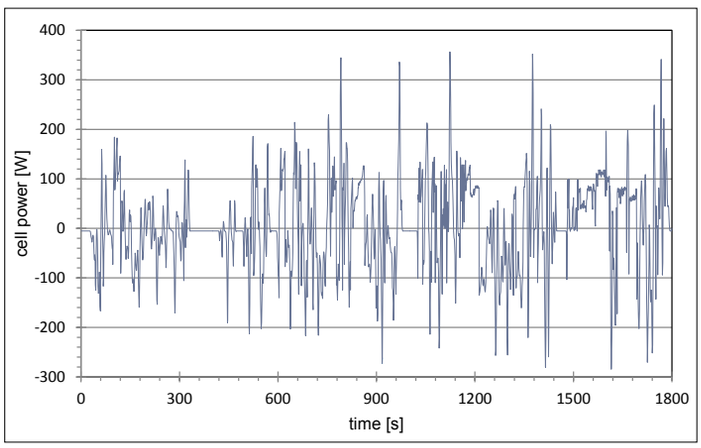

Fig. 1. Derived WLTC cell power profile versus time: positive values represent charging, negative values discharging.[6]

a lower discharge capacity of 3.79 Ah (cell 3) and 3.87 Ah (cell 4).

Cell 5 served as unstressed reference for microscopic analysis.

Capacity measurements were performed between power stress cycles in order to determine the discharge capacity of the cells. The characterization procedure started with a complete discharge of the cell to the discharge end voltage of 1.6 V. Then the cell was charged using the constant current–constant voltage procedure (1 C: voltage limit of 3.8 V, termination current of 0.22 A equivalent to 0.05 C) to determine the charge capacity. In order to obtain the discharge capacity the cell was discharged with a current of 0.88 A (0.2 C) to the end voltage of 1.6 V. Impedance spectroscopy (IS) was conducted on cell 1 in a frequency range from 1 mHz to 10 kHz. During the cycling experiments, the IS at 183 different aging stages was measured, one every 51 stress profiles. At each stage four spectra were recorded: at 20, 40, 60, and 80% SOC. All stress tests and characterization measurements were performed in a temperature-controlled safety chamber at 23 °C using the Maccor Series 4000 with a FRA 0355 setup.

3. Results and Discussion

3.1 *Discharge Capacity*

For standard applications end-of-life of batteries is usually defined to be reached when the capacity is reduced to 80% of their nominal discharge capacity.[7] With cycling according to the WLTC procedure cell 1 was fluctuating on each cycle between 42% and 100% SOC. It reached 80% of the nominal capacity after 8560 WLTC stress profiles (Fig. 2), corresponding to a vehicle-driven distance of 195'779 km. Cell 2 was cycled between 0% and 100% SOC with the average power of the WLTC procedure. End-of-life capacity of 80% was reached after 1175 cycles (Fig. 2).

The total energy throughput to reach the 80% nominal capacity was 284.2 kWh for cell 1 and 38.1 kWh for cell 2, respectively. This demonstrates that the total capacity throughput until end-of-life is reached strongly depends on stress profiles and is application specific. During the storage period at room temperature before stress cycling cells 3 and 4 lost about 15% of their nominal capacity. The comparably inferior performance of cells 3 and 4 can be explained by their storage time in a discharged state. This shows that the absolute cell capacity is not always a conclusive indicator for its state of health and over-discharged periods have to be considered when evaluating stress induced ageing and estimating residual lifetime. In conclusion, the WLTC profile was gentler compared to pure charge-discharge cycles with comparable power stresses, as performed with cells 2 to 4 (Table 1).

3.2 *Impedance Spectra*

Impedance spectra of cells 1 to 4 taken at 60% SOC are presented in Fig. 3. Spectra of cell 1 have been already published by Cuervo Reyes *et al.*[8] At medium frequencies an increase of the resistance Re(Z) with ageing is observed. At the initial state cells 1 and 2 show a typical RC-semicircle, which is attributed to the charge transfer resistance at the cathode-electrolyte interface and the current collector interfaces. Their shift to the right and up at the end of test is an indication of increased impedance of electrode contacts and electrolyte. Cells 3 and 4 show a different impedance characteristic already at the initial state because they were stored for long periods in a discharged state, which leads to decomposition of electrolyte and probably to dissolution of copper from the anode contact.

The low frequency end of the impedance is dominated by the concentration-driven Li-ion mass transport in the cathode, which for ideal diffusion should appear as a straight line with slope one.[9,10] A change of this slope with ageing has been reported and discussed within the constant phase element model[8] in which the increase of the slope of impedance is explained by sub-diffusive ion transport. The constant phase behavior has the form $Z = (i\omega)^{(\alpha/2-1)}$ for concentration-driven transport, and $Z = (i\omega)^{(\alpha-1)}$ for voltage-driven electronic transport with $\alpha = 0$ for perfect insulators and $\alpha = 1$ for perfect diffusive transport.

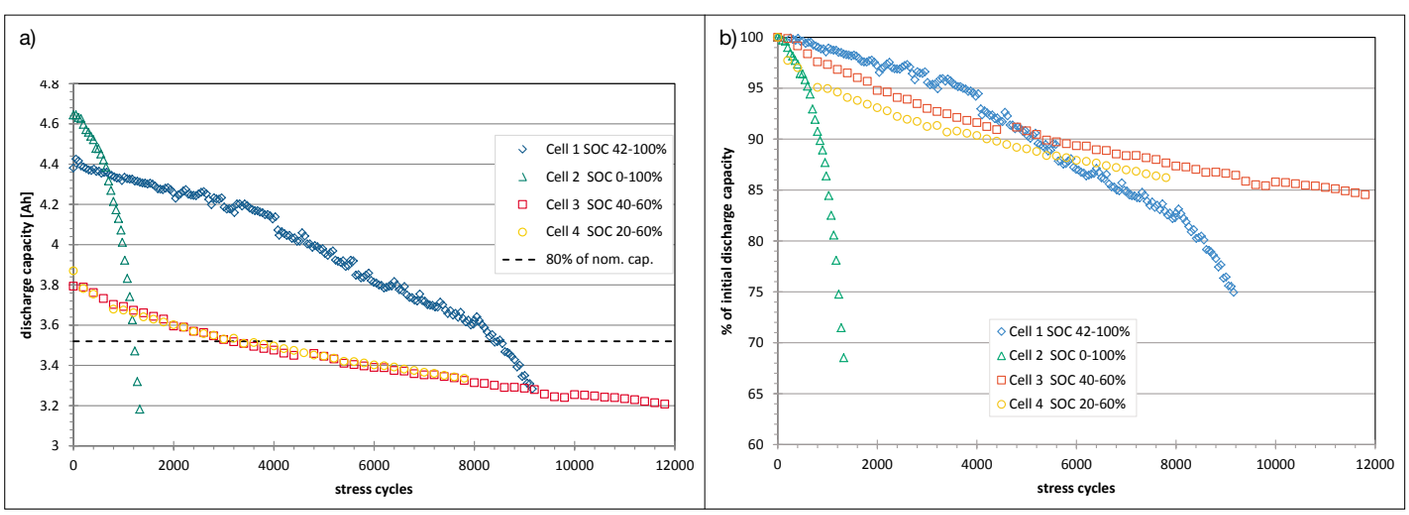

Fig. 2. Discharge capacity of the investigated cells as a function of the number of stress cycles or applied WLTC profiles, respectively, (a) absolute capacity, (b) normalized to 100% capacity at the beginning of stress cycles.

Table 1. Summary of stress cycle parameters until cells reached 3.52 Ah discharge capacity

	Charged [Ah]	Discharged [Ah]	Total [Ah]	Stress time [h]	Total Energy throughput [kWh]	# of cycles to 80% of nominal capacity (80% of 4.4Ah)
Cell 1	42426	42328	84754	4579	284.2	8560
Cell 2	5784	5780	11564	690	38.1	1175
Cell 3	2816	2816	5632	282	18.8	3200
Cell 4	5808	5808	11616	580	38.5	3300

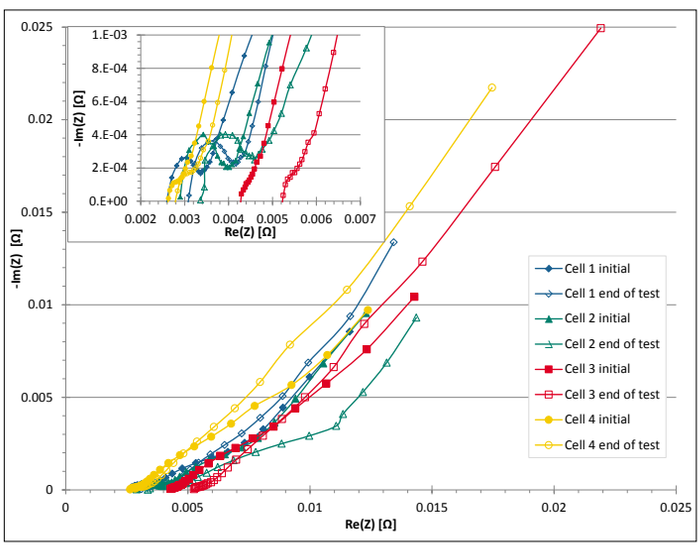

Fig. 3. Nyquist plot of the electric impedance of cells 1 to 4 at initial state and end of tests, taken at 60% SOC and in the frequency range from 1 mHz to 400 Hz. The insert in the upper left corner shows an expanded view of the lower left corner (medium frequency behavior).

Considering that Li-ion cells are complex systems composed of inhomogeneous materials with local deviations of ionic and electronic conductivity one cannot exclude from impedance spectra alone that electronic transport in the cathode can become the limiting factor at low frequencies, too.

3.3 *Microscopic Analysis*

To perform microscopic analysis cells 4 and 5 were opened, unrolled (Fig. 4), and samples of about 1.5 × 2.5 cm at selected positions have been extracted. The end faces of the samples were properly cut with a picosecond laser and afterwards polished with the Ga-beam of about 20 nA and 30 keV of a FEI Helios NanoLab 660 G3 UC DualBeam Ga-FIB/SEM microscope. For imaging and material analysis, an electron beam with secondary electron detection (SE) and EDX were used. High resolution ion beam imaging was done with a Zeiss Orion He-FIB with a specified spatial resolution of 0.35 nm.

Fig. 4. Opened cell 5 showing from outside to inside separator, cathode ($LiFePO_4$ – Al - $LiFePO_4$ stack), separator, anode (C – Cu - C stack).

An overview of the polished cross section showing a stack with anode, separator, cathode, and again separator is given in Fig. 5. To reduce material re-deposition during the FIB polishing process on the approximately 160 µm thick cross section, separate regions were polished from two opposite faces and combined in the split image of Fig. 5 for better visualization of layers and interfaces. Starting from the top of the polished cross section the carbon anode with interlaced copper, a separator with three layers (high-low-high density), the $LiFePO_4$ anode with interlaced aluminum, and again a separator with three layers at the bottom starting the next stack of the rolled topology of the cell can be identified. The copper and aluminum sheets of anode and cathode, respectively, are connected to the outside of the battery cell. In Fig. 6 an expanded view of the three-layered separator is given.

The carbon anode is irregularly structured with surface corrugated grains and voids with size of order 1 to 10 µm. At the interface of carbon and copper conductor (Fig. 7) strings of residual binder are shown. In He-ion images (expanded insert in upper-right corner of Fig. 7) particles

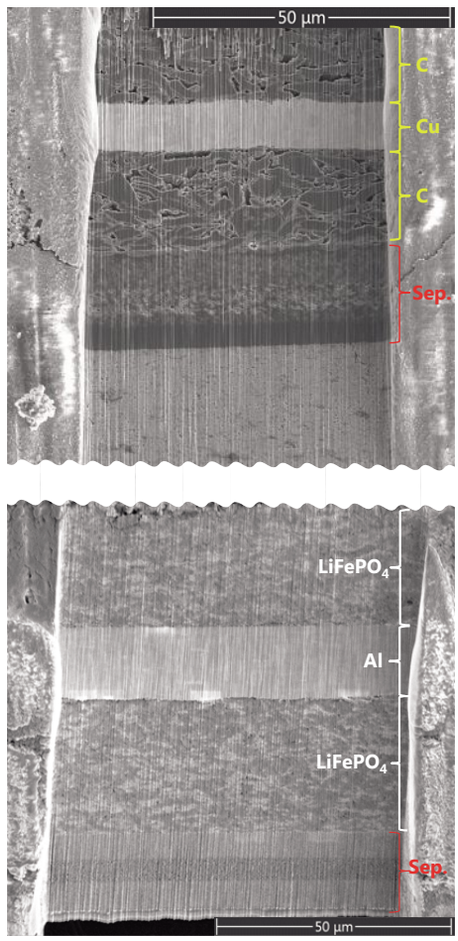

Fig. 5. SEM image of cross section of electrodes and separator of cell 4 prepared by picosecond laser ablation and polished by Ga-FIB. The vertical waterfall structure is an artefact of polishing.

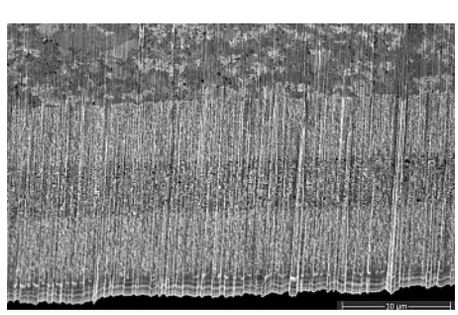

Fig. 6. SEM image of cross section of the 3-layered structure of the separator of cell 4.

with a size of about 10 nm at the surface of the carbon grains and the copper interface can be observed. They are also observed on cathode and separator surfaces. They may be explained by salt precipitation from the electrolyte and may have grown during the drying process.

In the $LiFePO_4$ cathode of cell 4 regions of enhanced density with a size of several microns are observed (Fig. 8). EDX analysis (Fig. 9) reveals that they contain an order of magnitude more carbon than on average, presumably added by the cell manufacturer to increase the conductivity of otherwise poorly conductive $LiFePO_4$

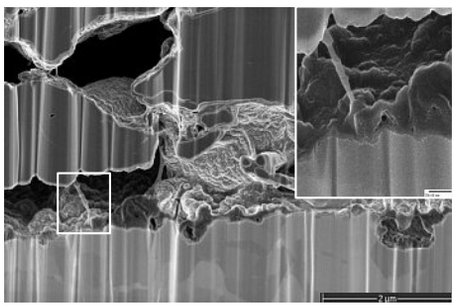

Fig. 7. SEM image of anode material at the copper interface of cell 4 showing the corrugated surface of the carbon particles and strings of binder. In the expanded view of a binder string taken with a He-FIB and displayed in the top-right corner the deposition of nanoparticles of about 10 nm diameter can be observed. Similar particle deposition is also observed at inner surfaces of separator and cathode material.

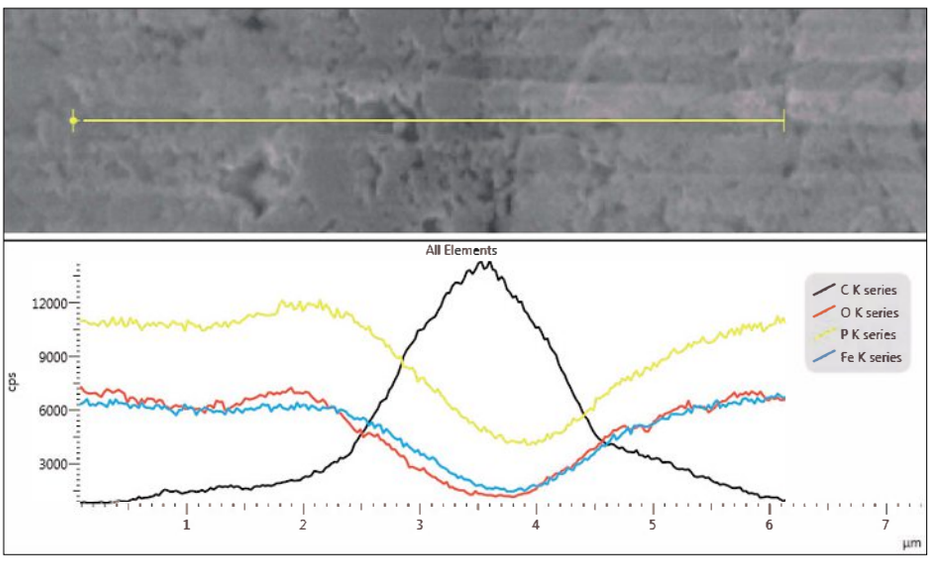

Fig. 9. EDX analysis of cell 4 along the indicated line (upper figure) showing high C content of compact areas of cathode material.

material. To estimate the influence of this inhomogeneous carbon distribution on cathode efficiency, further investigations are required.

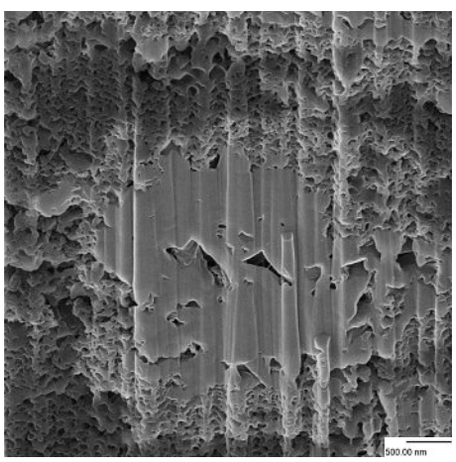

Fig. 8. He-FIB image of a compact area of the cathode.

At the interface in the cathode of $LiFePO_4$ and Al (Fig. 10) the formation of cavities at the few micrometer scale can be observed. In the expanded insert in the upper-right corner it is observed that for a large part of the cross section the cracking did not occur at the interface itself, but a few tens of nanometers into the $LiFePO_4$ cathode layer.

In conclusion the strong dependence of useful lifetime of $LiFePO_4$ batteries from stress profile, state of charge, and environmental conditions require quantitative

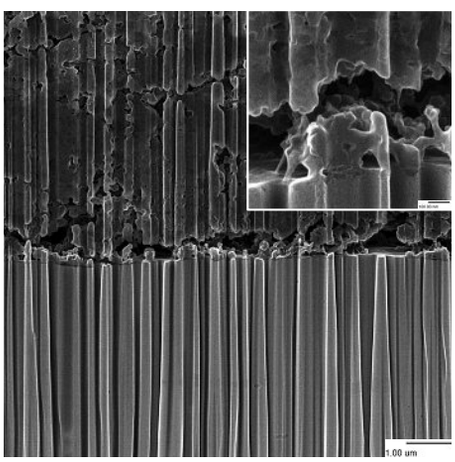

Fig. 10 He-FiB image of cathode aluminum interface of cell 4 showing cavity formation near the interface. The expanded view in the upper right corner demonstrates that cracking preferentially occurs not at the surface layer but in the cathode material.

estimations of the influence of the different material degradation processes of the complex battery system for efficient optimization. Microscopic analysis of stressed and unstressed cells combined with electronic and ionic transport modeling and finite element calculations may contribute to resolve some ambiguous interpretations of impedance spectroscopy data.

Acknowledgments

We thank D. Adams, R. Brönnimann, E. Cuervo-Reyes, M. Stiefel, C. Pecnik, and E. Stilp for their contributions to sample preparations, measurements, and discussions.

Received: August 10, 2015

[1] R. Hausbrand, G. Cherkashinin, H. Ehrenberg, M. Gröting, K. Albe, C. Hess, W. Jaegermann, *J. Mater. Sci. Eng. B* **2015**, *192*, 3.
[2] J. Vetter, P. Novák, M.R. Wagner, C. Veit, K.-C. Möller, J.O. Besenhard, M. Winter, M. Wohlfahrt-Mehrens, C. Vogler, A. Hammouche, *J. Power Sources* **2005**, *147*, 269.
[3] A. Barré, B. Deguilhem, S. Grolleau, M. Gérard, F. Suard, D. Riu, *J. Power Sources* **2013**, *241*, 680.
[4] E. M. Fellberg, Ph.D. Thesis Univ. Münster No. 10156, **2012**.
[5] T. Ott, C. Onder, L. Guzzella, *Energies* **2013**, *6*, 3571.
[6] Transport Division/World Forum for Harmonization of Vehicle Regulations (UN/ECE/WP29).
[7] IEC 62660-1, Secondary Lithium-Ion Cells for the Propulsion of Electric Road Vehicles, Part 1: Performance Testing, **2010**.
[8] E. Cuervo-Reyes, C. P. Scheller, M. Held, U. Sennhauser, *J. Electrochem. Soc.* **2015**, *162.8*, A1585.
[9] U. Tröltzsch, O. Kanoun, H.-R. Tränkler, *Electrochim. Acta* **2006**, *51.8*, 1664.
[10] J.R. Macdonald, E., Barsoukov 'Impedance spectroscopy: theory, experiment, and applications', Wiley, Hoboken, **2005**.